2024 IEEE/ASME International Conference on Advanced Intelligent Mechatronics (AIM)
July 15-19, 2024. Boston, MA, USA

Scanner with Reluctance Actuators for Tunable Motor Constant to Overcome Tradeoff

Atsuki Yamashita[1] and Shingo Ito[2]

***Abstract*— In a conventional scanner with an electromagnetic actuator for high-speed scanning motions with nanometer resolution, its motor constant needs to be determined in a tradeoff between the achievable speed and the motion precision due to noise from the inputs. To overcome the tradeoff, this paper proposes a scanner that integrates a pair of reluctance actuators for a tunable motor constant. Model-based analysis shows that the motor constant can be tuned by introducing a bias current, and the motion precision can be improved by decreasing the motor constant when a high force is unnecessary. To demonstrate the effectiveness, a laboratory setup is developed with motion control, achieving a high control bandwidth of about 300 Hz. Experimental results show that the motor constant of the proposed scanner can be decreased by a factor of 9, improving the positioning error from 16.7nm to 5.2 nm at a static point. The results successfully demonstrate the tuning function of the proposed scanner and its effectiveness on the motion precision.**

I. INTRODUCTION

High-precision motion is essential for high-precision imaging systems such as wafer scanners [1] and flat panel display (FPD) lithography systems [2], and atomic force microscopes [3]. In these systems, high-precision actuators typically accelerate a mover for scanning at a high constant speed with nanometer resolution. To further improve the throughput of these systems, a high-precision actuator with a larger force is required without impairing motion precision [4].

Lorentz actuators [5] are most commonly used high-precision electromagnetic actuators for motion with nanometer resolution, including voice coil actuators. Lorentz actuators generates a force proportional to their coil current for high linearity. Furthermore, their zero-stiffness property [5] is ideal to isolate disturbances transmitted from the stator for motion precision [6] [7]. However, Lorentz actuators have a disadvantage that their motor constant (force-to-current ratio) is relatively small [8]. To generate a large force, a large coil current is required, which wastes energy in the form of heat [9].

A large force can be generated by using actuators with reluctance force, such as reluctance actuators [10] and hybrid reluctance actuators (normal-stressed electromagnetic actuators) [11] [12]. Particularly, hybrid reluctance actuator (HRA) integrate a permanent magnet to generate an actuation force that is proportional to the coil current for high linearity and realize a motor constant that can be a few times larger than comparable Lorentz actuators [6]. To apply these actuators with reluctance force to practical applications, it is desired to improve their motion resolution. However, when input noise is taken into account, there exists a design tradeoff to determine a motor constant between the achievable force and motion resolution, as it is discussed in detail in Section IV.

For high-speed scanning motion with high resolution by overcoming the above-mentioned design tradeoff, this paper proposes a scanner with two identical reluctance actuators to tune a motor constant. It is to be maximized to generate a large force when the mover accelerates and deaccelerates, while the motor constant is minimized for high resolution during a high-speed scanning at a constant speed.

In this paper, development of the proposed scanner is presented to realize the desired motor-constant tunability. Furthermore, experiments are carried out to demonstrate the force-precision tradeoff and to validate the tunability to overcome it at a static point.

This paper is organized as follows. In Section II, the proposed scanner is described. In Section III, modeling of the system including a variable motor constants and dynamic model are discussed. Section IV describes the motor constant dilemma, which is a fundamental problem of conventional actuators. Section V describes the feedback control design with gain scheduling. Experimental results are presented and discussed in Section VI, and Section VII concludes the paper.

II. SYSTEM DESCRIPTION

Figure 1 shows a setup of the proposed scanner that uses a pair of reluctance actuators (Actuator 1 and Actuator 2) to tune a motor constant. Each reluctance actuator consists of an E-core and an I-core. They are made of laminated electric steel sheets to reduce eddy currents for energy efficiency. Coils are wound around the stators to generate magnetic fluxes. The I-cores are fixed to the mover. To laterally guide its motion, the mover is mounted onto an air bearing (A-101.050, PI, Karlsruhe, Germany), for high-precision motion without disturbances such as friction. For motion control, the lateral mover position is measured by an interferometer (IDS3010, attocube system, Haar, Germany) and an retroreflector (N-BK7, Edmund, Barrington, U.S.A.) is mounted onto the mover as the sensor target. The reluctance actuators' coils are connected to custom-made current amplifiers with current monitors. These amplifiers and the interferometers are connected to a rapid prototyping

*This work was supported by JSPS KAKENHI Grant Number JP22K14204.

[1]A. Yamashita is with Graduate School of Engineering, University of Fukui, 3-9-1 Bunkyo, Fukui, 910-8507, Japan ms230263@g.u-fukui.ac.jp

[2]S. Ito is with Department of Mechanical Engineering, University of Fukui, 3-9-1 Bunkyo, Fukui, 910-8507, Japan ito@u-fukui.ac.jp

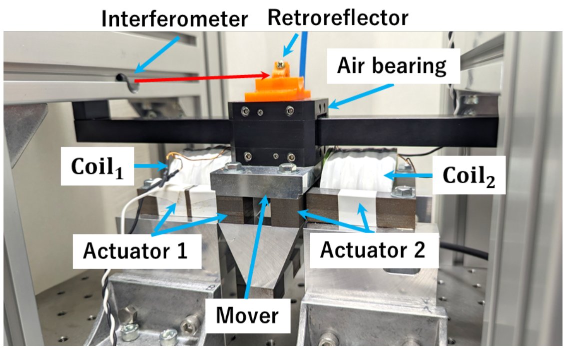

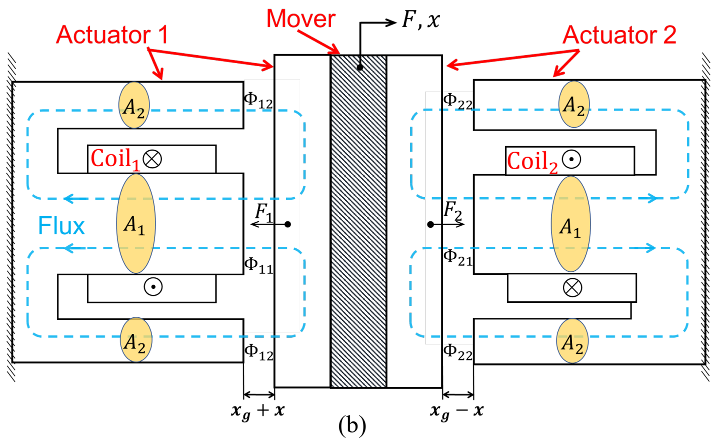

Fig. 1. Scanner with reluctance actuators with tunable motor constant. (a) Photograph of experimental setup. (b) Model of the pair of ruluctance actuators.

TABLE I
DESIGN PARAMETERS OF THE RELUCTANCE ACTUATORS

Parameter	Value	Description
x_g	1 mm	Air gap at $x = 0$.
N	600	Number of the coil windings. .
A_1	15 mm × 24 mm	Cross-section area of flux paths of the center gap.
A_2	15 mm × 12 mm	Cross-section area of flux paths of the side gaps.

control system (MicroLabBox, dSPACE GmbH, Paderborn, Germany), which runs at a sampling time of 40 kHz to implement control. Note that the proposed scanner has an advantage that it does not have a parasitic force unlike the first prototype [13].

III. System Analysis

To derive an actuation force and a dynamic model of the scanner, it is modeled by magnetic circuits [14], and it is assumed that the permeability of the electric steel sheets are sufficiently large in this section.

A. Model of the actuation force

As shown in Figure 1 (b), Actuator 1 and Actuator 2 have six airgaps. The airgaps at the center have a cross-sectional area of A_1, while the other side ones have a cross-sectional area of $A_2 = A_1/2$ by considering flux saturation. The reluctance of the center airgaps (R_{11} and R_{21}) and the side airgaps (R_{12} and R_{22}) are

$$R_{11} = \frac{x_g + x}{\mu_0 A_1} \ , \quad R_{12} = \frac{x_g + x}{\mu_0 A_2}, \tag{1}$$

$$R_{21} = \frac{x_g - x}{\mu_0 A_1} \ , \quad R_{22} = \frac{x_g - x}{\mu_0 A_2}, \tag{2}$$

where x_g, x, and μ_0 are the air gaps, the mover position, and the magnetic permeability in vacuum, respectively. The values of the parameters are shown in Table 1. Current I_1 and I_2 are applied to the left and right coils, respectively, to generate magnetic Φ_{11}, Φ_{12}, Φ_{21}, and Φ_{22} as shown Figure 1(b). From (1) and (2), they are given by applying Hopkinson's Law [5]:

$$\Phi_{11} = \frac{\mu_0 \ A_1 \ N \ I_1}{x_g + x} \ , \quad \Phi_{12} = \frac{\mu_0 \ A_2 \ N \ I_1}{x_g + x}, \tag{3}$$

$$\Phi_{21} = \frac{\mu_0 \ A_1 \ N \ I_2}{x_g - x} \ , \quad \Phi_{22} = \frac{\mu_0 \ A_2 \ N \ I_2}{x_g - x}, \tag{4}$$

where N is the number of the coil windings.

The force F_1 of Actuator 1 is calculated by using the Maxell stress tensor [15]:

$$F_1 = \frac{\Phi_{11}^2}{2\mu_0 A_1} + 2\,\frac{\Phi_{12}^2}{2\mu_0 A_2} = \frac{\Phi_{11}^2}{\mu_0 A_1} = \frac{\mu_0 A_1 N^2 I_1^2}{4(x_g + x)^2}. \tag{5}$$

Similarly, the force F_2 of Actuator 2 is given by

$$F_2 = \frac{\mu_0 A_1 N^2 I_2^2}{4(x_g - x)^2}. \tag{6}$$

For the capability to tune a motor constant, a bias current I_b and control current I_c are introduced as follows:

$$I_1 = I_b - I_c, \ I_2 = I_b + I_c. \tag{7}$$

Substituting (7) for (5) and (6), the total actuation force F is approximated by

$$F = \ F_2 - F_1 \approx \frac{\mu_0 A_1 N^2}{{x_g}^2} \ I_b \ I_c \ = \ K_M(I_b) I_c, \tag{8}$$

where the motor constant is

$$K_M = \frac{\mu_0 A_1 N^2}{{x_g}^2} \ I_b. \tag{9}$$

In the above equation, it is assumed that the mover moves in a small range ($x \approx 0$) for simplicity.

An advantage to introduce I_b is that the reluctance actuators can be linearized, such that F is proportional to I_c

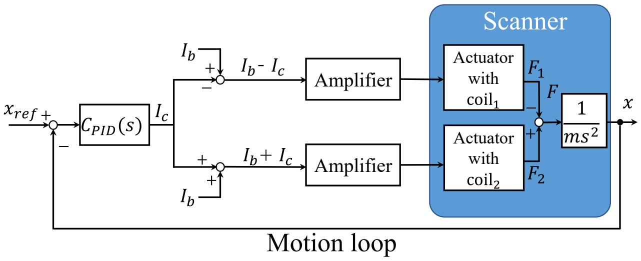

Fig. 2. Control block diagram of the scanner.

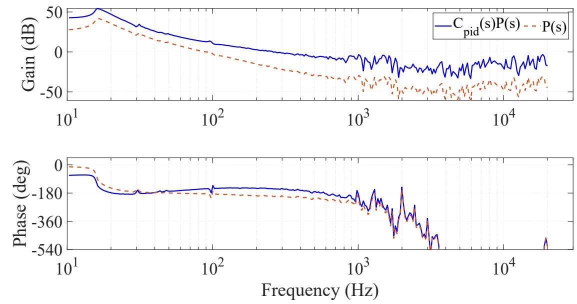

Fig. 3. Measured frequency response function of $P(s)$ from the control current I_c to the mover position x at I_b=0.1 A when sponges are inserted into airgaps, and an open-loop transfer function $C_{pid}(s)P(s)$ at I_b=0.1 A for control design.

for control [5]. More importantly, (9) shows that the motor constant K_M can be tuned in real time by tuning I_b. This feature is utilized to overcome the dilemma in Section IV.

B. Dynamic modeling

To demonstrate the force-precision tradeoff and the effectiveness of the motor-constant tunability at a static point, a feedback controller is designed in section V. For the purpose, the scanner is modeled by using an equation of motion about in:

$$F = K_M(I_b)\ I_c = m\ddot{x}, \tag{10}$$

where m is the mover mass. of 0.93 kg. Laplace transform of the above equation gives a transfer function of the plant

$$P(s) = \frac{x(s)}{I_c(s)} = \frac{K_M(I_b)}{ms^2}, \tag{11}$$

Figure 2 illustrates the derived model. Note that the modeling above is simplified to capture dynamics at relatively high frequency, which is sufficient to design a stable feedback controller for positioning at a static point in Section V. For high-speed scanning, more detailed modeling will be required (e.g., for feed forward control design), which is a part of future work.

C. Frequency response

For control design in Section V, a frequency response function (FRF) is measured. In the measurement, soft sponges are temporarily inserted into airgaps for stability without feedback control. Furthermore, by setting I_b to a small current of 0.1 A, the system is " frozen" for a linear system. The red lines in Figure 3 show the measured FRF. Around 13 Hz, a resonance is visible due to the sponges. However, at higher frequencies between 30 Hz and 1 kHz, a mass line with a slope of $-40\ dB/dec$ and a phase of about $-180°$ can be seen as moddeled in (11).

IV. Motor Constant Dilemma

Similar to (8), conventional high-precision electromagnetic actuators generate a force F that is proportional to the coil current I:

$$F = K_M\ I. \tag{12}$$

For a fast scanning motion, large F is required for high acceleration and deceleration. Since I is limited to prevent overheating, small K_M of Lorentz actuators is problematic. However, increasing K_M as realized by HRAs can generate a new problem when input noise is considered. The current I includes noise δI, due to measurement noise of current sensors in amplifiers and quantization noise of DACs and ADCs [16]. Consequently F includes noise $\delta F = K_M \delta I$ due to (12). When K_M is increased for a large acceleration, noise δF is also increased, impairing the motion precision. This implies that conventional actuators with fixed K_M cannot simultaneously realize a high force and a precise force. Consequently, K_M needs to be determined during system design in a trade off between the achievable acceleration and motion resolution [13], which is referred to as "motor constant dilemma" in this paper. To overcome the motor constant dilemma, the proposed scanner can adjust K_M in (8), which is to be increased for a large force during high acceleration and decreased for motion precision during scanning at a constant speed.

V. Control Design

A. Control design for plant at I_b=0.1 A

For experiments in Section VI to investigate the tunability of the motor constant and the positioning resolution at a static point, a feedback controller is designed. Since the measured FRF in Figure 3 has a phase of $-180°$, a tamed PID controller $C_{pid}(s)$ is used for I_b=0.1 A as shown in Figure 2 to provide a phase lead for closed-loop stability [5], as follows:

$$C_{pid}(s) \ = \ g_{pid}\frac{(s+\frac{\omega_c}{10})(3s+\omega_c)}{s(s+3\omega_c)}, \tag{13}$$

where g_{pid} and ω_c are the gain and the desired crossover frequency, respectively.

These parameters are adjusted to maximize closed-loop bandwidth. The blue lines in Figure 3 show a simulated open-loop transfer function when ω_c and g_{pid} are set to 400 Hz and 46.4 dB(= 208.9). It shows a phase margin of about 26 deg and a gain margin of about 6.4 dB for stability.

B. Gain scheduling

Since I_b is a function of the plant, the gain of the feedback controller needs to be adjusted according to the value of

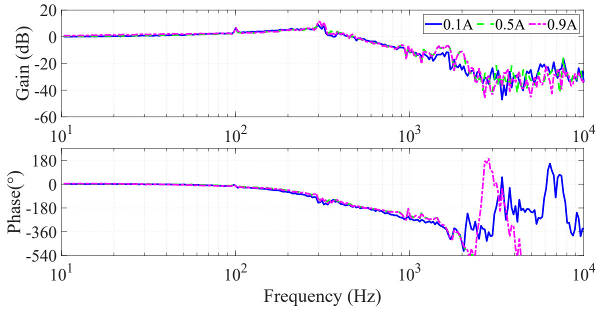

Fig. 4. Measured complementary sensitivity functions $T(s)$ from the position reference x_{ref} to the mover position x for bias current I_b=0.1 A, 0.5 A and 0.9 A.

I_b. Thus, a PID controller with gain-scheduling [17] [18] is implemented for stability with an arbitrary I_b by replacing g_{pid} in (13) by

$$g_{pid} = 208.9\frac{0.1}{I_b}. \quad (14)$$

This gain maintains the crossover frequency around 400Hz even when I_b varies.

C. Control validation

For validation of the designed and implemented controller with gain scheduling, The complementary sensitivity functions $T(s)$ from the position reference x_{ref} to the mover position x are measured at I_b=0.1 A, 0.5 A and 0.9 A. Figure 4 shows the results. The -3dB bandwidth varies in a small range between 552 Hz and 576 Hz, demonstrating successful implementation of the PID controller with gain-scheduling for a high closed-loop bandwidth and closed-loop stability.

VI. Experimental results

A. Tunability of motor constant

To evaluate the capability of the scanner to tune its motor constant, FRFs of the plant $P(s)$ in (11) are measured by varying I_b. Since the feedback controller stabilizes the scanner, the FRFs are measured in a closed loop, without the sponges. The results are shown in Figure 5, where mechanical resonances are visible at high frequencies of 1 kHz and higher. At low frequencies less than 50 Hz, the gain slope varies dependent on I_b, which may be due to the approximation for simplicity in (8). Approximately between 70 Hz and 1 kHz, a mass line with a slope of -40 dB/dec can be seen, and its gain depends on I_b, as modeled in (11).

To analyze the relation between the mass line and I_b in detail, the gain of each mass line at 300 Hz in Figure 5 is normalized by that of $I_b = 0.1\ A$ as the increase of the motor constant. The result in Figure 6 shows that the motor constant linearly increases with a slope of about one, which corresponds to the analytical model (11). More importantly, the motor constant increases by a factor of 9 by adjusting I_b, which successfully demonstrates the tuning capability of the proposed scanner.

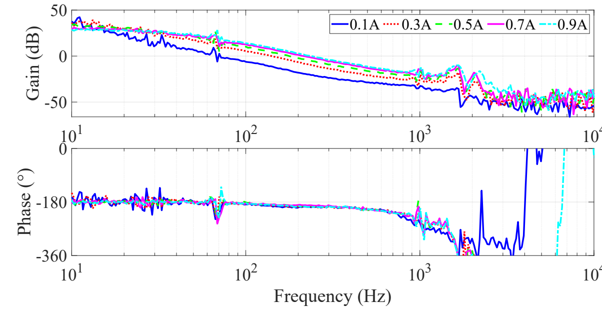

Fig. 5. Measured frequency response functions of plant $P(s)$ for each bias current I_b between 0.1 A and 0.9 A.

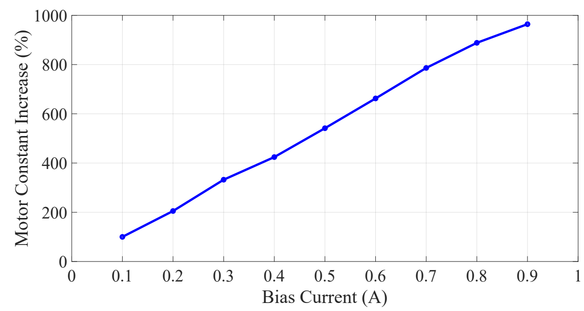

Fig. 6. Relation between the bias current and the motor constant.

B. Positioning resolution

To experimentally demonstrate the motor constant dilemma, motion resolution is measured at a static point by setting the position reference x_{ref} to 0 and by varying I_b between 0.1 A and 0.9 A. Figure 7 shows the results, where the motion resolution is evaluated by an RMS of a tracking error $e = x_{ref} - x$. The plot clearly shows that the tracking error gets larger by increasing I_b and the motor constant accordingly. Note that the plotted line is not straight but curved. This might be due to other disturbances such as floor vibrations, and they are more dominant when the motor constant is small. For further analysis in the time domain, the measured position x at I_b=0.1 A and 0.9 A are compared in Figure 8. When I_b is set to 0.9 A, the measured position shows a peak-to-peak value of 120 nm with an RMS of 16.7 nm. By decreasing I_b to 0.1 A, the peak-to-peak value is significantly reduced by a factor of about three to 40 nm with an RMS of 5.2 nm. Overall, the experimental results demonstrate that the motor constant dilemma exists and that the proposed scanner can tune its motor constant to adjust the motion resolution.

VII. Conclusion and future work

While a large motor constant of high-precision electromagnetic actuators is desired for high acceleration and deceleration, it can impair the motion resolution by increasing the influence of the noise included in the coil current. To overcome the motor constant dilemma, this paper proposed a scanner with reluctance actuators. The analytical models show that by introducing a bias current,

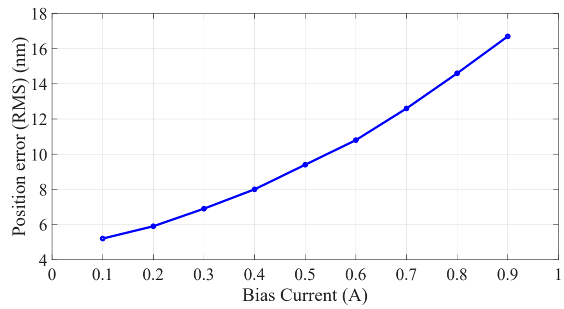

Fig. 7. Relation between the bias current I_b and the tracking error (RMS).

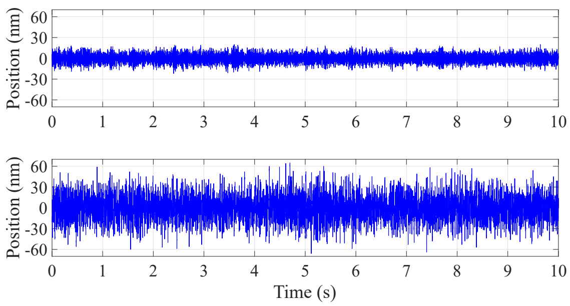

Fig. 8. Measured position x at the bias current I_b of (top) 0.1A and (bottom) 0.9A.

the scanner's motor constant and the plant gain can be tuned, and the actuation force can be linearized. To experimentally confirm the tunability, a PID controller with gain-scheduling is designed, such that the closed-loop -3 dB bandwidth is about 550 Hz. The experiments successfully validates that the proposed scanner can tune its motor constant up to a factor of 9, influencing the achievable motion resolution at a static point. Future work includes high-speed raster scanning by tuning the motor constant in real time for high precision.

References

[1] M. Heertjes, H. Butler, N. Dirkx, S. van der Meulen, R. Ahlawat, K. O'Brien, J. Simonelli, K.-T. Teng, and Y. Zhao, "Control of wafer scanners: Methods and developments," pp. 3686–3703, 2020.

[2] M. Hosek and J. T. Moura, "Advanced control techniques for semiconductor and flat panel display substrate handling robots," *IFAC Proceedings Volumes*, vol. 41, no. 2, pp. 6731–6738, 2008.

[3] P. Eaton and P. West, *Atomic Force Microscopy*. OUP Oxford, 2010.

[4] H. Butler, "Position control in lithographic equipment [applications of control]," *IEEE Control Systems Magazine*, vol. 31, no. 5, pp. 28–47, 2011.

[5] R. Munnig Schmidt, G. Schitter, A. Rankers, and J. van Eijk, *The Design of High Performance Mechatronics (3rd revised edition)*. IOS Press, 2020.

[6] A. Katalenic and P. van den Bosch, "Voltage based linearization of a reluctance actuator for high-precision applications," *IFAC Proceedings Volumes*, vol. 46, no. 5, pp. 170–176, 2013.

[7] S. Ito, S. Unger, and G. Schitter, "Vibration isolator carrying atomic force microscope's head," *Mechatronics*, vol. 44, pp. 32–41, 2017.

[8] N. H. Vrijsen, J. W. Jansen, and E. A. Lomonova, "Comparison of linear voice coil and reluctance actuators for high-precision applications," 2010.

[9] T. Tuma, W. Haeberle, H. Rothuizen, J. Lygeros, A. Pantazi, and A. Sebastian, "Dual-stage nanopositioning for high-speed scanning probe microscopy," *IEEE/ASME Transactions on Mechatronics*, vol. 19, no. 3, pp. 1035–1045, 2014.

[10] A. Katalenic, H. Butler, and P. P. J. van den Bosch, "High-precision force control of short-stroke reluctance actuators with an air gap observer," *IEEE/ASME Transactions on Mechatronics*, vol. 21, no. 5, pp. 2431–2439, 2016.

[11] S. Ito, S. Troppmair, B. Lindner, F. Cigarini, and G. Schitter, "Long-range fast nanopositioner using nonlinearities of hybrid reluctance actuator for energy efficiency," *IEEE Transactions on Industrial Electronics*, vol. 66, no. 4, pp. 3051–3059, 2019.

[12] X. Wang, Y. Meng, W.-W. Huang, L. Li, Z. Zhu, and L. Zhu, "Design, modeling, and test of a normal-stressed electromagnetic actuated compliant nano-positioning stage," *Mechanical Systems and Signal Processing*, vol. 185, p. 109753, 2023.

[13] S. Ito, L. Hu, and G. Schitter, "Development of an actuator with a variable motor constant for precision scanning motions," *Annual Meeting of JSPE Hokuriku Shin-etsu Branch, p. 17*, 2021.

[14] M. Kazimierczuk, *High-Frequency Magnetic Components*, 2014.

[15] E. P. Furlani, "Premanent magnet and electromechanical devices," *Academic press*, 2001.

[16] S. Letzter and N. Webster, "Noise in amplifiers," *IEEE Spectrum*, vol. 7, no. 8, pp. 67–75, 1970.

[17] V. Veselý and A. Ilka, "Gain-scheduled pid controller design," *Journal of Process Control*, vol. 23, no. 8, pp. 1141–1148, 2013.

[18] M.-S. Kim and J.-H. Kim, "Design of a gain scheduled pid controller for the precision stage in lithography," *International Journal of Precision Engineering and Manufacturing*, vol. 12, no. 6, pp. 993–1000, 2011.